RSC Advances

PAPER

View Article Online
View Journal | View Issue

Cite this: *RSC Adv.*, 2016, **6**, 22043

Pyrazino[2,3-*g*]quinoxaline-2,7-dione based π-conjugated polymers with affinity towards acids and semiconductor performance in organic thin film transistors†

Jesse Quinn, Chang Guo, Lewis Ko, Bin Sun, Yinghui He and Yuning Li*

Received 9th December 2015
Accepted 17th February 2016

DOI: 10.1039/c5ra26227e

www.rsc.org/advances

Pyrazino[2,3-*g*]quinoxaline-2,7-dione (**PQx**) was used as a building block for π-conjugated polymer semiconductors, which demonstrated a strong acid affinity by showing marked bathochromic shifts in their absorption spectra. These polymers exhibited semiconductor performance in organic thin film transistors (OTFTs). Copolymers of **PQx** and bithiophene exhibited electron-dominant ambipolar transport characteristics with electron mobilities of up to 4.28 × 10^{-3} cm^2 V^{-1} s^{-1} and hole mobilities of up to 5.22 × 10^{-4} cm^2 V^{-1} s^{-1}, while copolymers of **PQx** and thieno[3,2-*b*]thiophene exhibited hole-dominant ambipolar transport characteristics with hole mobilities of up to 4.82 × 10^{-2} cm^2 V^{-1} s^{-1} and electron mobilities of up to 3.95 × 10^{-3} cm^2 V^{-1} s^{-1}.

Introduction

Organic electronics have made great strides in recent decades. Certain characteristics of organic electronic devices such as flexibility and low-cost manufacturing make them ideal candidates for niche applications such as radio-frequency identification (RFID) tags, flexible displays, memory devices and sensors.[1–5] Organic thin film transistors (OTFTs) have been extensively studied as essential components of integrated circuits (ICs),[6,7] backplanes for displays,[8,9] memory devices,[10,11] and as chemo- and bio-sensors.[12–18]

Through rational structural design and optimization, polymer semiconductors based on the amide/imide-containing building blocks such as naphthalene diimide (NDI)[19] and derivatives,[20,21] diketopyrrolopyrrole (DPP),[22] isoindigo (IID)[23] and (3*E*,7*E*)-3,7-bis(2-oxoindolin-3-ylidene)benzo[1,2-*b*:4,5-*b*′]difuran-2,6(3*H*,7*H*)-dione (IBDF)[24] have exhibited high carrier mobilities in OTFTs. A recent work demonstrated that an OTFT sensor with an IID based-polymer showed promising sensitivity to heavy metals in both freshwater and saltwater, demonstrating the excellent environmental stability of amide/imide building blocks that are essential for sensor applications.[25]

Previously, we introduced an imide-containing building block, pyrimido[4,5-*g*]quinazoline-4,9-dione (**PQ**, Fig. 1),[26,27] for polymer semiconductors, which showed hole transport characteristics in OTFTs and strong response towards acids.[28] However, the backbones of these polymers are not very coplanar due to the steric repulsion between the *N*-alkyl side chains on the **PQ** unit and the neighbouring thiophene units, which would hamper the charge transport along the polymer backbone and through the interchain π–π stacks. In this study, we report an isomer of **PQ**, pyrazino[2,3-*g*]quinoxaline-2,7-dione (**PQx**, Fig. 1), which places the *N*-alkyl substituents at a greater distance from the neighbouring thiophene units, achieving a highly coplanar polymer backbone. Quinoxalin-2(1*H*)-one or pyrazininone (a half of the **PQx** structure) derivatives have been reported as candidates suitable as anti-tumor, antimicrobial, and antithrombotic agents.[28–32] For this reason, it is expected that **PQx**-based polymers may also exhibit activities towards various chemical and biological analytes allowing for applications as OTFT based chemo- and bio-sensors.[33–35]

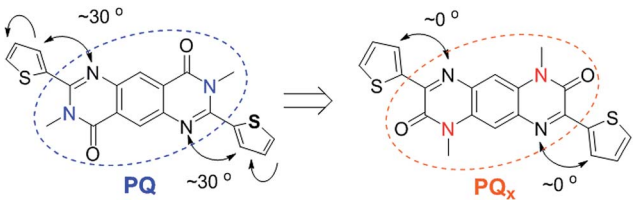

Fig. 1 Chemical structures of pyrimido[4,5-*g*]quinazoline-4,9-dione (**PQ**) and pyrazino[2,3-*g*]quinoxaline-2,7-dione (**PQx**).

Results and discussion

To the best of our knowledge, synthesis of the **PQx** moiety was only reported in one paper in 1970, where benzene-1,2,4,5-

Department of Chemical Engineering and Waterloo Institute of Nanotechnology, (WIN), University of Waterloo, 200 University Ave West, Waterloo, N2L 3G1, Canada. E-mail: yuning.li@uwaterloo.ca; Fax: +1-519-888-4347; Tel: +1-519-888-4567 ext. 31105

† Electronic supplementary information (ESI) available: Details of computer simulations, NMR, DSC, and addition OTFT data. See DOI: 10.1039/c5ra26227e

tetraamine and arylenediglyoxylates were condensed to form polymeric materials.[36] Due to the extremely low solubility of these polymers, no definite structural assignments were made. In this study, a similar synthetic procedure for the synthesis of quinoxalin-2(1*H*)-one compounds[37] is followed to synthesize the target 3,8-di(thiophen-2-yl)-1,6-dihydropyrazino[2,3-*g*]quinoxaline-2,7-dione (**PQx2T-H**) from 1,2,4,5-benzenetetramine tetrahydrochloride and 2-thiopheneglyoxylic acid (Scheme 1). A similar amount of the isomeric by-product, **iso-PQx2T-H**, is expected to form during the reaction. However, the crude product mixture is insoluble in any solvents and thus was used for the next step without further purification. *N*-Alkylation of the crude **PQx2T-H** was conducted using 11-(bromo-methyl)tricosane in the presence of K_2CO_3 in DMF at 130 °C to afford **PQx2T-24** in 9% yield. The alkylated by-product, **iso-PQx2T-24**, was probably produced based on the thin layer chromatography (TLC) analysis. However, this by-product could not be isolated from other impurities. Next, **PQx2T-24** was brominated with *N*-bromosuccinimide (NBS) to obtain **PQx2T-Br-24** in 64% yield. Polymers **PPQx2T-BT-24** and **PPQx2T-TT-24** were synthesized *via* Stille coupling polymerization of **PQx2T-Br-24** with 5,5′-bis(trimethylstannyl)-2,2′-bithiophene and 2,5-bis(trimethylstannyl)thieno[3,2-*b*]thiophene, respectively, and purified using Soxhlet extraction. Most of **PPQx2T-BT-24** (68%) was dissolved in refluxing chloroform, while 22% of this polymer was obtained by using 1,1,2,2-tetrachloroethane. Only the fraction extracted by chloroform was used for characterization. **PPQx2T-TT-24** showed much better solubility with 97% of it being extracted with chloroform. The number average molecular weight (M_n) and polydispersity index (PDI) were measured to be 24.6 kg mol^{-1} and 7.86 for **PPQx2T-BT-24** and 14.4 kg mol^{-1} and 2.05 for **PPQx2T-TT-24**, respectively (ESI†). Data were obtained using high-temperature gel-permeation chromatography (HT-GPC) at 140 °C with 1,2,4-trichlorobenzene as an eluent and polystyrene as standards. The GPC trace for **PPQx2T-BT-24** appears to be a trimodal distribution, which might be due to the aggregation of polymer chains that have been often observed for conjugated polymers.[38–40] As mentioned previously, **PPQx2T-BT-24** showed much poorer solubility than **PPQx2T-TT-24**, indicating a stronger aggregation tendency of the former. The thermal stability of these polymers was characterized using thermogravimetric analysis (TGA) and differential scanning calorimetry (DSC, ESI†). **PPQx2T-BT-24** showed good thermal stability with a 5% weight loss temperature ($T_{-5\%}$) at 325 °C, while **PPQx2T-TT-24** showed slightly higher thermal stability with a $T_{-5\%}$ at 332 °C. No noticeable endo- or exothermic transitions were observed on their differential scanning calorimetry (DSC) diagrams (ESI†).

A computational study was conducted using the density functional theory (DFT) with the B3LYP/6-31G(d) level of theory under tight convergence to investigate the geometry, molecular energy levels, and electron distributions of a simple 2,7-dithienyl-substituted **PQx** molecule, **PQx2T-Me** (Fig. 2). The optimized geometry results revealed that the **PQx** unit is coplanar and there is no twisting between the flanking thiophenes and the **PQx** unit. The lowest unoccupied molecular orbital (LUMO) and highest occupied molecular orbital (HOMO) wavefunctions are evenly distributed throughout the molecule. The LUMO and HOMO energy levels of **PQx2T-Me** were calculated to be −2.75 eV and −5.53 eV, respectively. The LUMO energy level of **PQx2T-Me** is much lower than that of **PQ2T-Me** (−1.97 eV),[28] indicating **PQx** is a stronger electron acceptor than **PQ**. To investigate the polymer geometry and molecular energy levels, the dimer of **PQx2T-BT-Me** and **PQx2T-TT-Me** were simulated (ESI†). The LUMO and HOMO energy levels were calculated to be −2.95 eV and −4.90 eV for **PQx2T-BT-Me** and −2.99 eV and −4.96 eV for **PQx2T-TT-Me**, respectively. For both **PQx2T-BT-Me** and **PQx2T-TT-Me**, the LUMO wavefunctions are evenly distributed across the dimer. However, the HOMO wavefunctions appear largely distributed on the thiophene and thienothiophene moieties and only slightly scattered on the **PQx** moiety. The results suggest that

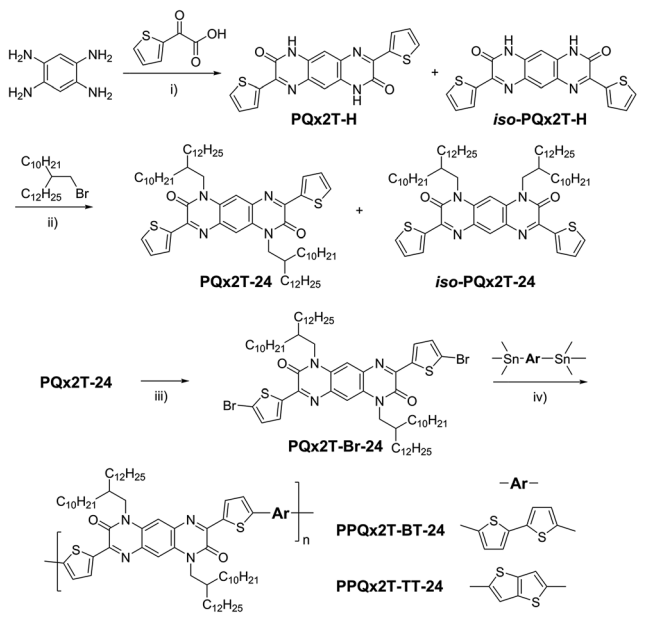

Scheme 1 The synthetic route to PPQx2T-BT-24 and PPQx2T-TT-24 polymers. Reagents and conditions: (i) acetic acid/reflux/overnight; (ii) K_2CO_3/DMF/130 °C; (iii) NBS/chloroform; (iv) $Pd_2(dba)3$/P(*o*-tolyl)$_3$/chlorobenzene/130 °C.

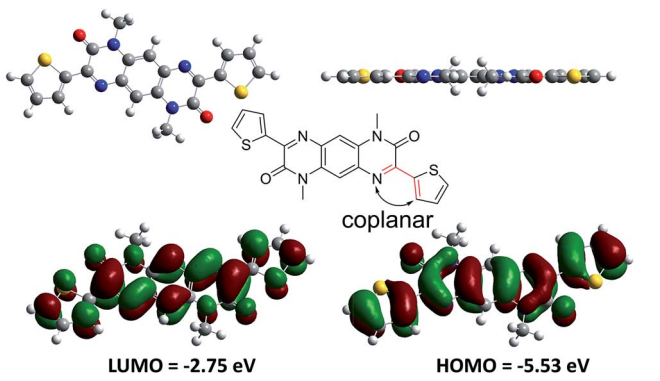

Fig. 2 Optimized geometry and HOMO and LUMO energy levels for PQx2T-Me obtained by DFT calculations at the B3LYP/6-31G(d) level of theory.

the HOMO energy levels for both dimers are mostly influenced by the thiophene and/or thienothiophene units. The dihedral angles between the **PQx** unit and thiophene units in **PQx2T-BT-Me** were <1°. However, greater twisting was observed between thiophene units with dihedral angles ranging from 6 to 8°. **PQx2T-TT-Me** was nearly coplanar with dihedral angles < 1° throughout the thiophene and thienothiophene units.

The surface morphology of the polymer thin films was characterized with atomic force microscopy (AFM) (Fig. 3). The polymer thin films were prepared under the same conditions as those used for the OTFT devices. In the AFM images of the **PPQx2T-BT-24** films annealed at 100, 150 and 200 °C, smooth surfaces with a low root mean squared roughness (R_q) of 0.5 nm were observed with very little difference. At 250 °C, the polymer thin film appears rougher with an increase of R_q to 1.1 nm. Under scrutiny, all **PPQx2T-BT-24** films are comprised of tiny grains, which is in agreement with its poor crystallinity verified by the X-ray diffractometry (XRD) (see below). On the other hand, the 100 °C-annealed **PPQx2T-TT-24** film shows distinct worm-like grains, indicative of its higher crystallinity. With increasing annealing temperature, the worm-like grains disappeared and pinholes formed concurrently. Layered structures comprising large pinholes are observed for the 250 °C-annealed film, which might cause the degraded OTFT performance at this annealing temperature.

The polymer thin films, which were prepared similarly as those for the OTFTs and AFM measurement, were subject to XRD measurement to study their crystallinity and molecular organization (ESI†). At all annealing temperatures (100, 150, 200 and 250 °C), **PPQx2T-BT-24** thin films showed no obvious diffraction peaks. In contrast, **PPQx2T-TT-24** thin film annealed at 100 °C exhibited a clear primary (100) diffraction peak at $2\theta = 3.68°$, which corresponds to a d-spacing distance of 2.40 nm. When the annealing temperature was increased to 150 °C, the (100) peak shifted slightly to $2\theta = 4.00°$ (d-spacing = 2.21 nm) accompanied by the appearance of a secondary (200) diffraction peak at $2\theta = 7.84°$, indicating that long range ordering formed.[41] At an annealing temperature of 200 °C, the intensity of both (100) and (200) peaks further increased and shifted to $2\theta = 3.92°$ (d-spacing = 2.25 nm) and $2\theta = 7.72°$, respectively. Further increasing the annealing temperature to 250 °C resulted in a decrease of intensity for the (100) peak and a decrease in the d-spacing to 2.21 nm ($2\theta = 4.00°$). However, the (200) peak became stronger and a tertiary (300) diffraction peak at $2\theta = 11.52°$ can be seen. Transmission XRD measurements were also performed using polymer flakes (ESI†). **PPQx2T-BT-24** and **PPQx2T-TT-24** showed strong (100) peaks at $2\theta = 3.31°$ and 3.63°, which correspond to the inter-lamellar distances of 2.67

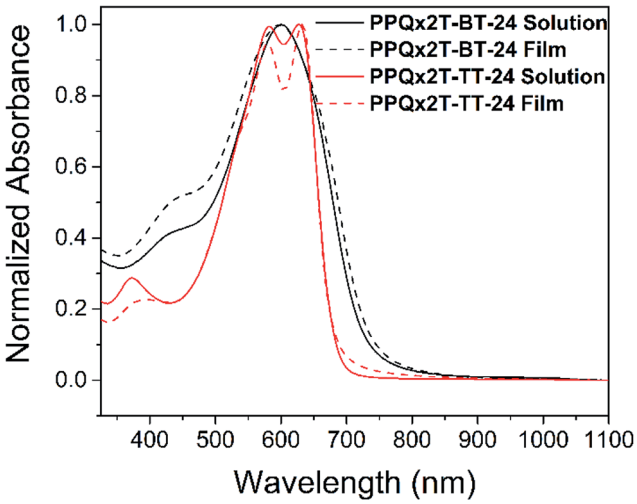

Fig. 4 UV-Vis-NIR absorption spectra of PPQx2T-BT-24 and PPQx2T-TT-24 in chloroform and as-cast films on glass substrates.

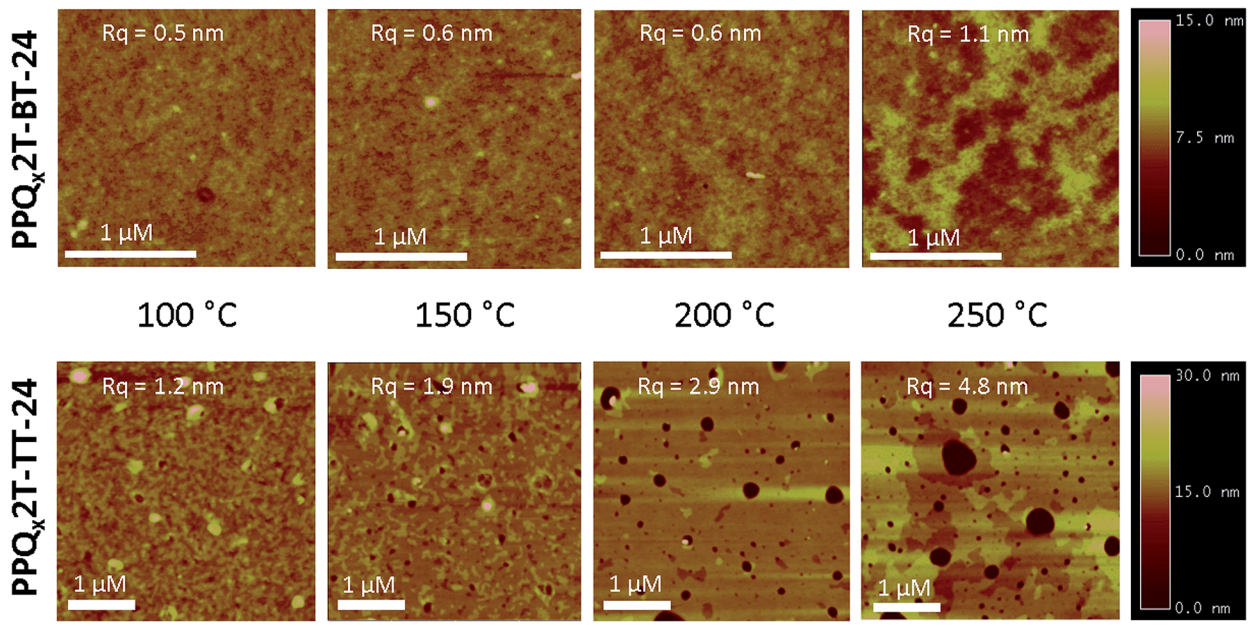

Fig. 3 AFM images of PPQx2T-BT-24 (2 μm × 2 μm) and PPQx2T-TT-24 (4 μm × 4 μm) films annealed at different temperatures.

nm and 2.43 nm, respectively. The hump centred at $2\theta = 23.58°$ observed for **PPQx2T-BT-24** could be assigned to the (010) peak originating from the co-facial π–π distance of adjacent polymer backbones,[42] which was calculated to be 0.38 nm. In comparison, a much stronger (010) peak was observed for **PPQx2T-TT-24** at $2\theta = 25.39°$ corresponding to a π–π distance of 0.35 nm. Thus, the higher crystallinity and a shorter π–π distance could be accounted for the higher charge mobility observed for **PPQx2T-TT-24**.

The frontier energy levels of these polymers were determined from the oxidation and reduction onset potentials on their thin film cyclic voltammetry (CV) (ESI†). The HOMO and LUMO energy levels of **PPQx2T-BT-24** are −5.54 eV and −3.59 eV, respectively. **PPQx2T-TT-24** has a same HOMO energy level of −5.54 eV, but a slightly higher LUMO energy level of −3.52 eV. The electrochemical band gaps are thus 1.95 eV for **PPQx2T-BT-24** and 2.01 eV for **PPQx2T-TT-24**. The greater electrochemical band gaps than the optical bandgaps are possibly caused by the large exciton binding energy that is typical of π-conjugated polymers.[22]

The UV-Vis-NIR absorption properties of **PPQx2T-BT-24** and **PPQx2T-TT-24** in chloroform and in thin films are shown in Fig. 4. In solution, **PPQx2T-BT-24** showed a broad featureless absorption profile with the maximum absorption wavelength (λ_{max}) to be 600 nm while a similar absorption profile and λ_{max} of 598 nm were observed with the film. **PPQx2T-TT-24** showed clearly two major peaks in both solution and film absorption profiles. The λ_{max} in solution appeared at 627 nm along with a slightly weaker peak at 582 nm. From solution to film, positions of these two peaks (at 632 nm and 576 nm) changed very little. The optical band gaps of **PPQx2T-BT-24** and **PPQx2T-TT-24** calculated from the onset absorption wavelengths of their thin films are ~1.66 eV and ~1.82 eV, respectively. Compared to its analogous **PQ** polymer **PPQ2T-BT-24**, which has an optical

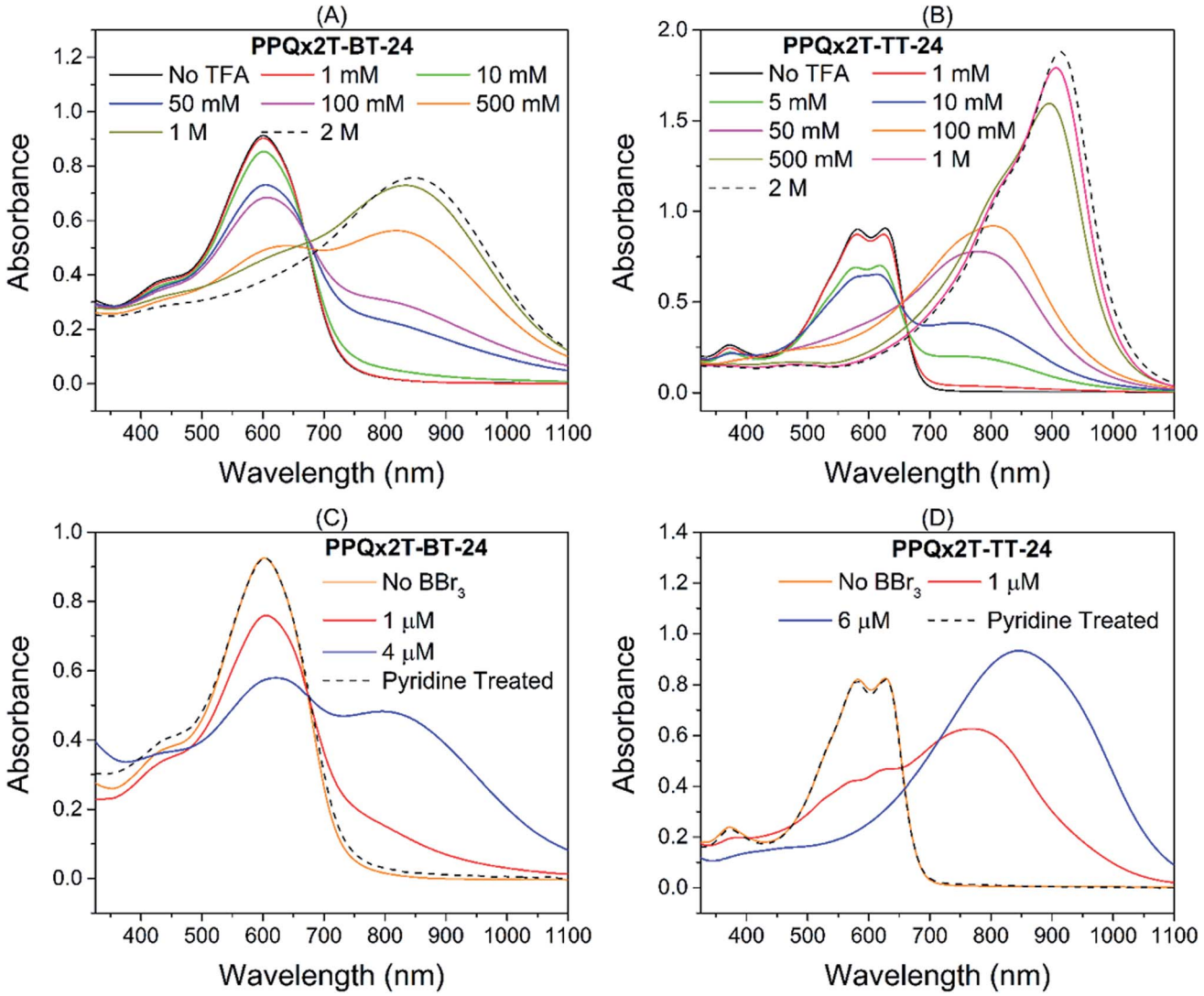

Fig. 5 (A) and (C) show the UV-Vis-NIR absorption spectra of **PPQx2T-BT-24** in chlorobenzene with various concentrations of TFA, and BBr_3, respectively; (B) and (D) show the UV-Vis-NIR absorption spectra of **PPQx2T-TT-24** in chlorobenzene with various concentrations of TFA and BBr_3, respectively. The measurements were conducted under nitrogen with a molar concentration of the polymer repeat unit at ~1×10^{-5} M.

band gap of 2.03 eV, **PPQx2T-BT-24** has a much narrower band gap because **PQx** is a stronger electron acceptor than **PQ**, which resulted in more efficient intramolecular donor-to-acceptor charge transfer, and a more coplanar backbone.

As with **PQ**-based polymers,[28] the basic 1,6-pyridyl nitrogen atoms of **PQx** are expected to allow the **PQx**-based polymers to interact strongly with acids. Similar behaviour has been reported for conjugated polymers and small molecules incorporating pyridine moieties[43,44] and benzothiadiazoles.[45–51] In contrast, azulene-based conjugated polymers and small molecules, which do not contain a basic site, have also shown noteworthy responses to various acids.[47,48,51] In all cases reversible bathochromic shifts in the absorption maxima occur with some cases reaching near infrared (NIR).[48,49,51] To elucidate the acid effects of these **PQx** polymers, trifluoroacetic acid (TFA), which has a pK_a of -0.25,[48] was first tested. As shown in Fig. 5A, **PPQx2T-BT-24** exhibited a slight decrease in absorbance at a TFA concentration as low as 1 mM. With increasing TFA concentration, the λ_{max} bathochromically shifted and the long wavelength tail intensified. At 500 mM TFA, the λ_{max} appeared at ~840 nm. Further increasing the TFA concentration caused a bathochromic shift in the new λ_{max} peak. At 2 M TFA, near the solubility limit for TFA in chlorobenzene, very little spectral change occurred and a largest λ_{max} of 846 nm was reached, which corresponds to a bathochromic shift of 246 nm from that of the solution without TFA. In the case of **PPQx2T-TT-24**, a slight decrease in absorption also started at 1 mM TFA (Fig. 5B). A new λ_{max} peak appeared at ~780 nm, similar to **PPQx2T-BT-24**, but at a lower TFA concentration (50 mM) and a shorter wavelength. This new λ_{max} peak bathochromically shifted up to 804 nm at 100 mM TFA. Surprisingly, the peak at 804 nm disappeared and a very intense peak appeared at ~900 nm as the TFA concentration increased to 500 mM. At 2 M TFA, the λ_{max} shifted to 914 nm, which corresponds to a bathochromic shift of 287 nm from that of the solution without TFA.

The effect of boron tribromide (BBr_3), a strong Lewis acid, on the absorption spectra of **PPQx2T-BT-24** (Fig. 5C) and **PPQx2T-TT-24** (Fig. 5D) was also studied. Both polymers at a BBr_3 concentration of 1 μM show absorption spectra similar to those observed for TFA at a concentration of 50 mM, indicating a much stronger interaction of BBr_3 with both polymers than that of TFA. At a BBr_3 concentration of 4 μM, **PPQx2T-BT-24** bathochromically shifted with a λ_{max} of 621 nm accompanied by the appearance of a strong absorption peak at 796 nm, which appears to be similar to that observed in the TFA solution at 500 mM. At a BBr_3 concentration beyond 4 μM, precipitates formed, which are assumed to be the polymer–BBr_3 complexes. For **PPQx2T-TT-24**, at a BBr_3 concentration of 6 μM, which is the maximum BBr_3 concentration without formation of precipitates, the λ_{max} bathochromically shifted to 846 nm, which is comparable to that observed for the TFA solution at 500 mM. In either case, with the addition of pyridine the original spectra of the pristine polymers could be completely recovered (Fig. 5C and D).

To reveal if the polymers have amplified sensitivity towards acids, the UV-Vis-NIR spectra of the monomer compound **PQx2T-24** solutions with various concentrations of TFA were measured. **PQx2T-24** showed a significant change at 25 mM TFA (Fig. 6). At 50 mM TFA, a broad featureless absorption peak with a λ_{max} of 516 nm was observed. There was little change as the TFA concentration was increased up to 100 mM. With a higher TFA concentration of 1 M, three well-defined peaks at 473 nm, 505 nm, and 542 nm (λ_{max}) appeared. Further increasing the TFA concentration to 2 M, the absorption profile remained the same, but the overall intensity increased. The overall bathochromic shift from the absence of TFA to 2 M of TFA is ~88 nm. **PPQx2T-TT-24** clearly demonstrates an amplification effect since this polymer exhibited a dramatic spectra change at a much lower TFA concentration of ~1–5 mM than **PQx2T-24**. On other hand, it appears that **PPQx2T-BT-24** has a similar sensitivity to TFA (at ~10–50 mM) compared to **PQx2T-24**. The reason for the dramatically differed responses to acids observed for these two polymers is unclear. The basicity of the 1,6-nitrogen atoms in **PQx** in these two polymer should be similar because they have similar HOMO energy levels. As aforementioned, **PPQx2T-BT-24** might form chain aggregates in solution, which would hinder the access of TFA molecules to the polymer chains inside the aggregates, resulting in the low sensitivity of this polymer.

PPQx2T-BT-24 and **PPQx2T-TT-24** were evaluated as channel semiconductors in bottom-gate, bottom-contact (BGBC) OTFT devices fabricated on dodecyltrichlorosilane (DDTS) modified SiO_2/Si wafer substrates. Both polymers showed ambipolar charge transport characteristics with **PPQx2T-BT-24** being electron-dominant and **PPQx2T-TT-24** being hole-dominant (Fig. 7, S22, and Table S1†). The electron-dominant transport behaviour of **PPQx2T-BT-24** is most likely due to its slightly lower LUMO energy level than that of **PPQx2T-TT-24**, which facilitated electron injection and stabilized electron

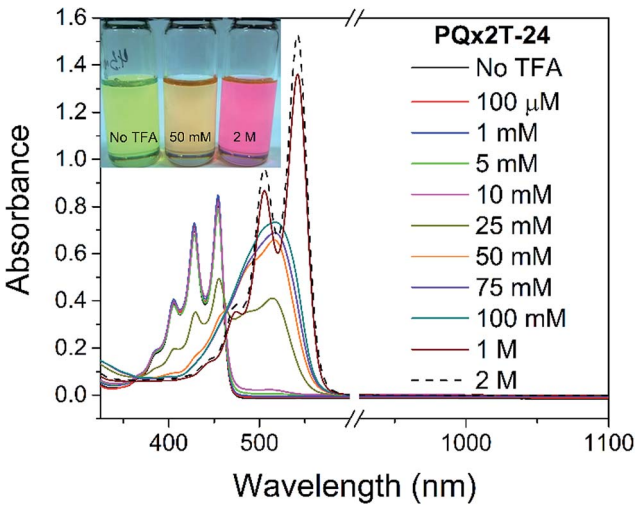

Fig. 6 The UV-Vis-NIR absorption spectra and photos of PQx2T-24 in chlorobenzene with various concentrations of TFA until little variations were observed. The measurements were conducted under nitrogen with a molar concentration at ~1×10^{-5} M. Photos of neutral and pronated PQx2T-24 (left: neutral in chlorobenzene; middle: protonated with 50 mM TFA; right: protonated with 2 M TFA).

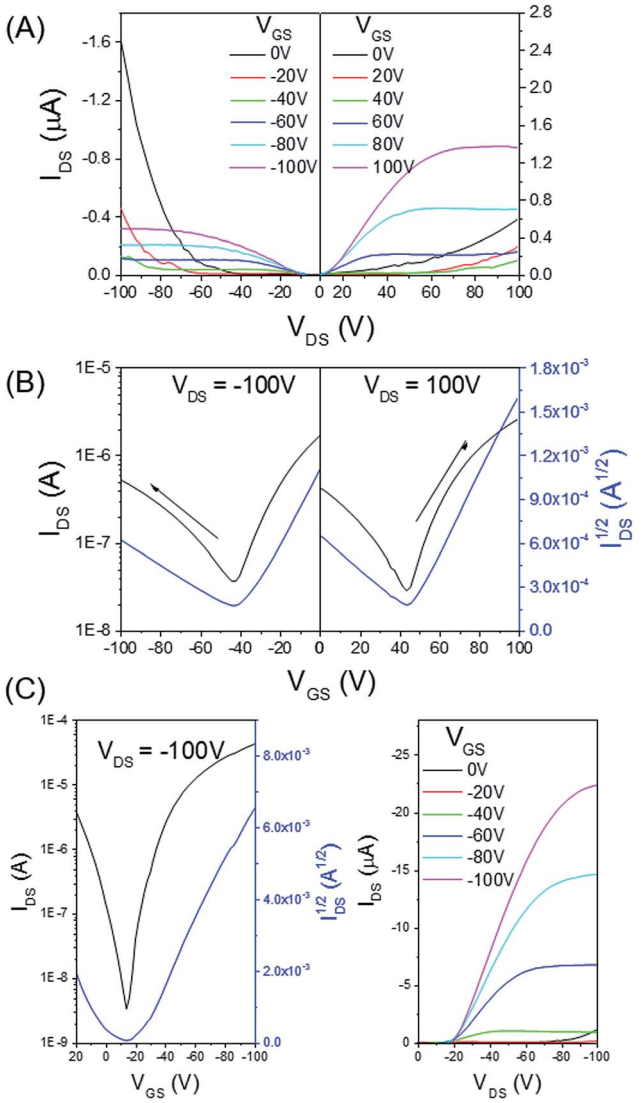

Fig. 7 Output (A) and transfer (B) curves of OTFT devices with **PPQx2T-BT-24** thin films annealed at 200 °C. Likewise, the output and transfer curves (B) of OTFT devices with **PPQx2T-TT-24** thin films annealed at 200 °C. Device dimensions: channel width (W) = 1000 μm; channel length (L) = 30 μm.

transport.[52–54] For devices based on **PPQx2T-BT-24**, the best performance was observed at 200 °C with the highest hole mobility of 5.22×10^{-4} cm^2 V^{-1} s^{-1} (5.04×10^{-4} cm^2 V^{-1} s^{-1} in average) and the highest electron mobility of 4.28×10^{-3} cm^2 V^{-1} s^{-1} (3.97×10^{-3} cm^2 V^{-1} s^{-1} in average). At a higher annealing temperature of 250 °C, both hole and electron mobilities decreased. For **PPQx2T-TT-24**, the highest hole mobility of 4.82×10^{-2} cm^2 V^{-1} s^{-1} (3.79×10^{-2} cm^2 V^{-1} s^{-1} in average) and the highest electron mobility of 3.95×10^{-3} cm^2 V^{-1} s^{-1} (3.12×10^{-3} cm^2 V^{-1} s^{-1} in average) were achieved also at the annealing temperature of 200 °C. The electron transport characteristics of devices with **PPQx2T-TT-24** started to appear only at a very high V_{GS} of >60 V in the n-channel operation mode (Fig. S22 and Table S1†). Both polymers showed decreased mobilities at a higher annealing temperature of 250 °C due to the deteriorated film morphology.

Conclusions

We report two polymers, **PPQx2T-BT-24** and **PPQx2T-TT-24**, based on the new building block, pyrazino[2,3-*g*]quinoxaline-2,7-dione (**PQx**). These polymers showed dramatic bathochromic shifts in their UV-Vis-NIR absorption spectra in the presence of trifluoroacetic acid and the Lewis acid boron tribromide. In OTFTs, **PPQx2T-BT-24** exhibited electron-dominant ambipolar transport characteristics with hole mobilities of up to 5.22×10^{-4} cm^2 V^{-1} s^{-1} and electron mobilities reaching 4.28×10^{-3} cm^2 V^{-1} s^{-1}. **PPQx2T-TT-24** exhibited hole-dominant ambipolar transport characteristics with hole mobilities of up to 4.82×10^{-2} cm^2 V^{-1} s^{-1} and electron mobilities of up to 3.95×10^{-3} cm^2 V^{-1} s^{-1}. Our preliminary results demonstrate that **PQx** is a promising new building block for polymer semiconductors for OTFTs that can be used for chemo- and bio-sensors.

Experimental

Materials and instrumentation

All chemicals were purchased from commercial sources and used without further purification. 11-(Bromomethyl)tricosane (C_{24}-Br) was synthesized using a method previously reported.[55] GPC measurements were performed on a Malvern SEC system using 1,2,4-trichlorobenzene as eluent and polystyrene as standards at 140 °C. TGA measurements were carried out on a TA Instruments Q500 at a temperature ramping rate of 10 °C min^{-1} under nitrogen. DSC measurements were carried out on a TA Instruments Q2000 at a temperature ramping rate of 20 °C min^{-1} under nitrogen. UV-Vis-NIR absorption spectra were obtained on a Thermo Scientific GENESYS™ 10S VIS spectrophotometer. Polymer solutions containing an acid were prepared by adding an intended amount of acid (TFA or BBr_3) in chlorobenzene under nitrogen. The molar concentration of the pyrazino[2,3-*g*]quinoxaline-2,7-dione (**PQx**) units of the polymer was kept at $\sim 1 \times 10^{-5}$ M. CV experiments were carried out on a CHI600E electrochemical analyser using an Ag/AgCl reference electrode and two Pt disk electrodes as the working and counter electrodes in a 0.1 M tetrabutylammonium hexafluorophosphate solution in anhydrous acetonitrile at a scan rate of 50 mV s^{-1}. Ferrocene was used as the reference, which has a HOMO energy level of −4.8 eV.[56] NMR spectra were recorded on a Bruker DPX 300 MHz spectrometer with chemical shifts relative to the residual chloroform in the deuterated solvent (7.26 ppm for ^{1}H NMR and 77 ppm for ^{13}C NMR). Reflection X-ray diffraction (XRD) diagrams of polymer thin films (~40 nm) spin-coated on dodecyltrichlorosilane-modified SiO_2/Si substrates and annealed at 100, 150, 200, and 250 °C for 30 min in nitrogen were obtained using a Bruker D8 Advance powder diffractometer with Cu Kα radiation (λ = 0.15406 nm). Transmission XRD measurements were carried out on a Bruker Smart 6000 CCD 3-circle D8 diffractometer with a Cu Kα (Rigaku) X-ray source (λ = 0.15406 nm) using polymer flakes stacked between two Mylar film substrates. AFM images were taken on polymer thin films spin-coated on the dodecyltrichlorosilane modified SiO_2/Si substrates with a Dimension 3100 scanning probe microscope. DFT calculations through

Gaussian 09 Revision D.01 (ref. 57) using the B3LYP/6-31G(d) level of theory under tight convergence were conducted to investigate the geometry, molecular energy levels, and electron distributions for the model compounds.

Synthesis of 3,8-di(thiophen-2-yl)-1,6-dihydropyrazino[2,3-*g*]quinoxaline-2,7-dione (PQx2T-H)

A 100 mL two-neck round-bottom flask was charged with 1,2,4,5-benzenetetramine tetrahydrochloride (1.1 g, 3.92 mmol), 2-thiopheneglyoxylic acid (1.2 g, 7.84 mmol) and acetic acid (80 mL). The mixture was then refluxed for 16 h. Subsequently, the reaction mixture was cooled to room temperature, added to water, filtered and washed with methanol to afford a yellow/brown solid (0.84 g, 56%). Due to its poor solubility, this product was used for the next step without further purification. An isomeric by-product, **iso-PQx2T-H**, is expected to form with a similar yield to that of **PQx2T-H** and present in this crude product.

Synthesis of 1,6-bis(2-decyltetradecyl)-3,8-di(thiophen-2-yl)-1,6-dihydropyrazino[2,3-*g*]quinoxaline-2,7-dione (PQx2T-24)

A 100 mL two-neck round-bottom flask was charged with the crude **PQx2T-H** (0.81 g, 2.2 mmol) and potassium carbonate (1.49 g, 10.8 mmol) and purged with argon. *N*,*N*-Dimethylformamide (DMF) (24 mL) was added and the reaction mixture was heated to 80 °C and stirred for 1 h before 11-(bromomethyl)tricosane (4.49 g, 10.8 mmol) was added. The reaction mixture was stirred at the same temperature for an additional 48 h. After cooling, the reaction mixture was extracted with dichloromethane and the separated organic phase was washed with water. The combined organic phases were dried and the solvent was removed. The residue was purified by column chromatography using 33% dichloromethane in hexanes to give a yellow liquid, which was treated with isopropanol three times to afford a yellow solid as the target product **PQx2T-24** (0.21 g, 9%). Based on the TLC analysis, a spot similar to that of **PQx2T-24** in size was observed, which could be the isomeric by-product, **iso-PQx2T-24** (Scheme 1), produced by alkylation of **iso-PQx2T-H** present in the crude starting material. However, **iso-PQx2T-24** could not be isolated by column chromatography due to its similar polarity to that of other impurities.

Data for **PQx2T-24** follows. ^{1}H-NMR (300 MHz, $CDCl_3$) δ 8.40 (s, 2H), 8.31 (d, $J = 3.8$ Hz, 2H), 7.59 (d, $J = 5.1$ Hz, 2H), 7.21 (t, $J = 4.5$ Hz, 2H), 4.62 (d, $J = 5.3$ Hz, 4H), 2.00 (br, 2H), 1.71–1.15 (m, 80H), 0.87 (t, $J = 6.5$ Hz, 12H). ^{13}C-NMR (75 MHz, $CDCl_3$) δ 154.23, 142.47, 140.75, 138.80, 137.78, 131.52, 130.96, 128.28, 124.19, 70.22, 37.74, 32.08, 31.86, 30.16, 29.85, 29.81, 29.52, 27.06, 22.85, 14.29. MS (ESI^+) $[M + H]^+$: 1051.

Synthesis of 3,8-bis(5-bromothiophen-2-yl)-1,6-bis(2-decyltetradecyl)-1,6-dihydropyrazino[2,3-*g*]quinoxaline-2,7-dione (PQx2T-Br-24)

A 100 mL two-neck round-bottom flask was charged with **PQx2T-24** (0.18 g, 0.17 mmol) and chloroform (7 mL). The reaction mixture was cooled to 0 °C and *N*-bromosuccinimide (NBS) (0.064 g, 0.36 mmol) was added. The reaction mixture was gradually warmed to room temperature. After stirring overnight in the absence of light, the reaction mixture was washed with a sodium sulfite solution and water, and dried over sodium sulfate. Purification using column chromatography with a mixture of 20% dichloromethane in hexanes afforded an orange solid (0.13 g, 64%). ^{1}H-NMR (300 MHz, $CDCl_3$) δ 8.35 (s, 2H), 8.03 (d, $J = 4.1$ Hz, 2H), 7.16 (d, $J = 4.1$ Hz, 2H), 4.61 (d, $J = 5.6$ Hz, 4H), 2.00 (s, 32H), 1.65–1.17 (m, 80H), 0.87 (t, $J = 6.2$ Hz, 12H). ^{13}C-NMR (75 MHz, $CDCl_3$) δ 153.74, 142.26, 141.14, 138.43, 137.54, 131.84, 131.60, 124.12, 119.17, 70.34, 68.90, 37.68, 32.09, 31.85, 30.20, 29.88, 29.84, 29.53, 27.09, 22.85, 14.27. HRMS (ESI^+) calculated for $C_{66}H_{104}Br_2N_4O_2S_2$ $(M + H)^+$: 1207.5996 found 1207.6046.

Synthesis of PPQx2T-BT-24

To a 25 mL Schlenk flask, **PQx2T-Br-24** (101.3 mg, 0.084 mmol), 5,5′-bis(trimethylstannyl)-2,2′-bithiophene (41.3 mg, 0.084 mmol) and tri(*o*-tolyl)phosphine (P(*o*-tolyl)$_3$) (2.1 mg, 0.007 mmol) were charged. After degassing and refilling argon three times, chlorobenzene (3 mL) and tris(dibenzylideneacetone)-dipalladium ($Pd_2(dba)_3$) (1.5 mg, 0.002 mmol) were added. The reaction mixture was stirred at 130 °C for 72 h. Upon cooling to room temperature, the reaction mixture was poured into methanol (100 mL). The precipitate was collected by filtration and subject to Soxhlet extraction with acetone, hexanes, and chloroform successively. Upon removal of solvent *in vacuo*, the chloroform extract gave 70 mg (68%) of **PPQx2T-BT-24**. Further extraction with 1,1,2,2-tetrachloroethane dissolved the remaining polymer, which gave 22 mg (21%) of the less soluble fraction upon removal of solvent *in vacuo*. Only the chloroform-extracted fraction was used for characterization. ^{1}H-NMR spectrum is provided in ESI.†

Synthesis of PPQx2T-TT-24

To a 25 mL Schlenk flask, **PQx2T-Br-24** (67.0 mg, 0.055 mmol), 2,5-bis(trimethylstannyl)-thieno[3,2-*b*]thiophene (25.6 mg, 0.084 mmol) and P(*o*-tolyl)$_3$ (1.3 mg, 0.004 mmol) were charged. After degassing and refilling argon three times, chlorobenzene (2 mL) and $Pd_2(dba)_3$ (1.0 mg, 0.001 mmol) were added. The reaction mixture was stirred at 130 °C for 72 h. Upon cooling to room temperature, the reaction mixture was poured into methanol (100 mL). The precipitate was collected by filtration and subjected to Soxhlet extraction with acetone, hexanes, and chloroform successively. Upon removal of solvent *in vacuo*, the chloroform extract gave **PPQx2T-TT-24**. Yield: 63 mg (97%). ^{1}H-NMR spectrum is provided in ESI.†

Fabrication and characterization of organic thin film transistors (OTFTs)

A bottom-gate, bottom-contact (BGBC) configuration was used for all OTFT devices. The device fabrication procedure is as follows. A heavily n^{++}-doped SiO_2/Si wafer with ~300 nm-thick SiO_2 was patterned with gold source and drain pairs by conventional photolithography and thermal deposition techniques. Next, the substrate was treated with O_2-plasma followed by cleaning with acetone and isopropanol *via* an ultra-sonicating bath. Then the substrate was placed in a solution of

dodecyltrichlorosilane in toluene (10 mg mL^{-1}) at room temperature for 20 min followed by washing with toluene and drying under a nitrogen flow. Subsequently a polymer solution in chloroform (5 mg mL^{-1}) was spin-coated onto the substrate at 3000 rpm for 60 s to give a polymer film (~40 nm), which was further subject to thermal annealing at various temperatures for 30 min in a glove box. All the OTFT devices have a channel length (L) of 30 μm and a channel width (W) of 1000 μm.

Devices were characterized in the same glove box using an Agilent B2912A Semiconductor Analyser. The hole and electron mobilities are calculated in the saturation regime according to the following equation:

$$I_{DS} = \left(\frac{WC_i}{2L}\right)\mu(V_G - V_{th})^2$$

where I_{DS} is the drain–source current, μ is the charge carrier mobility, C_i is the capacitance per unit area of the dielectric (11.6 nF cm^{-2}), W (1000 μm) and L (30 μm) are OTFT channel width and length, V_G is the gate voltage and V_{th} is the threshold voltage.

Acknowledgements

Financial support of this work by the Natural Sciences and Engineering Research Council (NSERC) of Canada (Discovery Grant #402566-2011) is acknowledged.

Notes and references

1 C. D. Dimitrakopoulos and P. R. L. Malenfant, *Adv. Mater.*, 2002, **14**, 99–117.
2 H. Yan, Z. Chen, Y. Zheng, C. Newman, J. R. Quinn, F. Dötz, M. Kastler and A. Facchetti, *Nature*, 2009, **457**, 679–686.
3 B. Peng and P. K. L. Chan, *Org. Electron.*, 2014, **15**, 203–210.
4 L. Liang, T. Fukushima, K. Nakamura, S. Uemura, T. Kamata and N. Kobayashi, *J. Mater. Chem. C*, 2014, **2**, 879–883.
5 S. P. White, K. D. Dorfman and C. D. Frisbie, *Anal. Chem.*, 2015, **87**, 1861–1866.
6 Y. Takeda, Y. Yoshimura, Y. Kobayashi, D. Kumaki, K. Fukuda and S. Tokito, *Org. Electron.*, 2013, **14**, 3362–3370.
7 S. Jacob, S. Abdinia, M. Benwadih, J. Bablet, I. Chartier, R. Gwoziecki, E. Cantatore, A. H. M. van Roermund, L. Maddiona, F. Tramontana, G. Maiellaro, L. Mariucci, M. Rapisarda, G. Palmisano and R. Coppard, *Solid-State Electron.*, 2013, **84**, 167–178.
8 S. Steudel, K. Myny, S. Schols, P. Vicca, S. Smout, A. Tripathi, B. van der Putten, J.-L. van der Steen, M. van Neer, F. Schütze, O. R. Hild, E. van Veenendaal, P. van Lieshout, M. van Mil, J. Genoe, G. Gelinck and P. Heremans, *Org. Electron.*, 2012, **13**, 1729–1735.
9 G. S. Ryu, J. S. Kim, S. H. Jeong and C. K. Song, *Org. Electron.*, 2013, **14**, 1218–1224.
10 Y.-C. Chiu, T.-Y. Chen, C.-C. Chueh, H.-Y. Chang, K. Sugiyama, Y.-J. Sheng, A. Hirao and W.-C. Chen, *J. Mater. Chem. C*, 2014, **2**, 1436–1446.
11 Y.-C. Chiu, T.-Y. Chen, Y. Chen, T. Satoh, T. Kakuchi and W.-C. Chen, *ACS Appl. Mater. Interfaces*, 2014, **6**, 12780–12788.
12 M. E. Roberts, S. C. B. Mannsfeld, N. Queraltó, C. Reese, J. Locklin, W. Knoll and Z. Bao, *Proc. Natl. Acad. Sci. U. S. A.*, 2008, **105**, 12134–12139.
13 P. Stoliar, E. Bystrenova, S. D. Quiroga, P. Annibale, M. Facchini, M. Spijkman, S. Setayesh, D. de Leeuw and F. Biscarini, *Biosens. Bioelectron.*, 2009, **24**, 2935–2938.
14 P. Lin and F. Yan, *Adv. Mater.*, 2012, **24**, 34–51.
15 W.-Y. Chou, Y.-S. Lin, L.-L. Kuo, S.-J. Liu, H.-L. Cheng and F.-C. Tang, *J. Mater. Chem. C*, 2013, **2**, 626–632.
16 J. Liao, S. Lin, K. Liu, Y. Yang, R. Zhang, W. Du and X. Li, *Sens. Actuators, B*, 2014, **203**, 677–682.
17 C. Liao, C. Mak, M. Zhang, H. L. W. Chan and F. Yan, *Adv. Mater.*, 2015, **27**, 676–681.
18 T.-P. Huynh, P. S. Sharma, M. Sosnowska, F. D'Souza and W. Kutner, *Prog. Polym. Sci.*, 2015, **47**, 1–25.
19 J. Shao, G. Wang, K. Wang, C. Yang and M. Wang, *Polym. Chem.*, 2015, **6**, 6836–6844.
20 L. M. Kozycz, C. Guo, J. G. Manion, A. J. Tilley, A. J. Lough, Y. Li and D. S. Seferos, *J. Mater. Chem. C*, 2015, **3**, 11505–11515.
21 W. Chen, J. Zhang, G. Long, Y. Liu and Q. Zhang, *J. Mater. Chem. C*, 2015, **3**, 8219–8224.
22 Y. Li, S. P. Singh and P. Sonar, *Adv. Mater.*, 2010, **22**, 4862–4866.
23 T. Lei, Y. Cao, Y. Fan, C. J. Liu, S. C. Yuan and J. Pei, *J. Am. Chem. Soc.*, 2011, **133**, 6099–6101.
24 Z. Yan, B. Sun and Y. Li, *Chem. Commun.*, 2013, **49**, 3790–3792.
25 O. Knopfmacher, M. L. Hammock, A. L. Appleton, G. Schwartz, J. Mei, T. Lei, J. Pei and Z. Bao, *Nat. Commun.*, 2014, **5**, 2954.
26 J. Quinn, E. Jin and Y. Li, *Tetrahedron Lett.*, 2015, **56**, 2280–2282.
27 J. Quinn, C. Guo, B. Sun, A. Chan, Y. He, E. Jin and Y. Li, *J. Mater. Chem. C*, 2015, **3**, 11937–11944.
28 S. A. Galal, S. H. M. Khairat, F. A. F. Ragab, A. S. Abdelsamie, M. M. Ali, S. M. Soliman, J. Mortier, G. Wolber and H. I. El Diwani, *Eur. J. Med. Chem.*, 2014, **86**, 122–132.
29 S. A. Galal, A. S. Abdelsamie, S. M. Soliman, J. Mortier, G. Wolber, M. M. Ali, H. Tokuda, N. Suzuki, A. Lida, R. A. Ramadan and H. I. El Diwani, *Eur. J. Med. Chem.*, 2013, **69**, 115–124.
30 S. N. Khattab, S. A. H. Abdel Moneim, A. A. Bekhit, A. M. El Massry, S. Y. Hassan, A. El-Faham, H. E. Ali Ahmed and A. Amer, *Eur. J. Med. Chem.*, 2015, **93**, 308–320.
31 S. A. Galal, A. S. Abdelsamie, H. Tokuda, N. Suzuki, A. Lida, M. M. ElHefnawi, R. A. Ramadan, M. H. E. Atta and H. I. El Diwani, *Eur. J. Med. Chem.*, 2011, **46**, 327–340.
32 R. Liu, Z. Huang, M. G. Murray, X. Guo and G. Liu, *J. Med. Chem.*, 2011, **54**, 5747–5768.
33 J. T. Mabeck and G. G. Malliaras, *Anal. Bioanal. Chem.*, 2005, **384**, 343–353.
34 C. Liao and F. Yan, *Polym. Rev.*, 2013, **53**, 352–406.
35 C. Liao, M. Zhang, M. Y. Yao, T. Hua, L. Li and F. Yan, *Adv. Mater.*, 2014, 1–35.

36 G. Rabilloud and B. Sillion, *Bull. Soc. Chim. Fr.*, 1970, 4052–4057.
37 J. Guillon, J. Louchahi-Raoul, M. Boulouard, P. Dallemagne, M. Daoust and S. Rault, *Pharm. Pharmacol. Commun.*, 1998, **4**, 319–324.
38 Y. Li, G. Vamvounis and S. Holdcroft, *Chem. Mater.*, 2002, **14**, 1424–1429.
39 H. Zhou, L. Yang, S. Liu and W. You, *Macromolecules*, 2010, **43**, 10390–10396.
40 Y. Li, P. Sonar, S. P. Singh, M. S. Soh, M. van Meurs and J. Tan, *J. Am. Chem. Soc.*, 2011, **133**, 2198–2204.
41 Y. He, C. Guo, B. Sun, J. Quinn and Y. Li, *Polym. Chem.*, 2015, **6**, 6689–6697.
42 M. J. Winokur, D. Spiegel, Y. Kim, S. Hotta and A. J. Heeger, *Synth. Met.*, 1989, **28**, 419–426.
43 P. Zalar, Z. B. Henson, G. C. Welch, G. C. Bazan and T.-Q. Nguyen, *Angew. Chem., Int. Ed.*, 2012, **51**, 7495–7498.
44 P. Zalar, M. Kuik, Z. B. Henson, C. Woellner, Y. Zhang, A. Sharenko, G. C. Bazan and T.-Q. Nguyen, *Adv. Mater.*, 2014, **26**, 724–727.
45 G. C. Welch, R. Coffin, J. Peet and G. C. Bazan, *J. Am. Chem. Soc.*, 2009, **131**, 10802–10803.
46 G. C. Welch and G. C. Bazan, *J. Am. Chem. Soc.*, 2011, **133**, 4632–4644.
47 T. Tang, G. Ding, T. Lin, H. Chi, C. Liu, X. Lu, F. Wang and C. He, *Macromol. Rapid Commun.*, 2013, **34**, 431–436.
48 T. Tang, T. Lin, F. Wang and C. He, *Polym. Chem.*, 2014, **5**, 2980.
49 T. Tang, H. Chi, T. Lin, F. Wang and C. He, *Phys. Chem. Chem. Phys.*, 2014, **16**, 20221.
50 E. Poverenov, N. Zamoshchik, A. Patra, Y. Ridelman and M. Bendikov, *J. Am. Chem. Soc.*, 2014, **136**, 5138–5149.
51 T. Tang, T. Lin, F. Wang and C. He, *J. Phys. Chem. B*, 2015, **119**, 8176–8183.
52 D. M. de Leeuw, M. M. J. Simenon, A. R. Brown and R. E. F. Einerhand, *Synth. Met.*, 1997, **87**, 53–59.
53 T. D. Anthopoulos, G. C. Anyfantis, G. C. Papavassiliou and D. M. de Leeuw, *Appl. Phys. Lett.*, 2007, **90**, 122105.
54 H. Yan, Z. Chen, Y. Zheng, C. Newman, J. R. Quinn, F. Dötz, M. Kastler and A. Facchetti, *Nature*, 2009, **457**, 679–686.
55 X. Guo and M. D. Watson, *Org. Lett.*, 2008, **10**, 5333–5336.
56 J. Pommerehne, H. Vestweber, W. Guss, R. F. Mahrt, H. Bässler, M. Porsch, J. Daub, H. Bassler, M. Porsch and J. Daub, *Adv. Mater.*, 1995, **7**, 551–554.
57 M. J. Frisch, *et al.*, Gaussian 09, 2009, see ESI† for the full citation.